Study of the influence of water vapour and carbon dioxide dilution on flame structure of swirled methane/oxygen-enriched air flames

Alexis Vandel, J.P. Chica Cano, S. de Persis, G. Cabot

Study of the influence of water vapour and carbon dioxide dilution on flame structure of swirled methane/oxygen-enriched air flames

A. Vandel[1], J.P. Chica Cano[1,2], S. de Persis[2,*], G. Cabot[1]

Affiliations

[1]CORIA, CNRS, UMR 6614, INSA de Rouen, Campus du Madrillet - BP 8, 76801 Saint Etienne du Rouvray cedex 2, France.

[2]ICARE, CNRS, UPR3021, Université d'Orléans, 1C, avenue de la recherche scientifique, 45071 Orléans cedex 2, France.

**Corresponding author: Stéphanie de Persis, stephanie.de_persis@cnrs-orleans.fr*

Abstract

In this work, the effect of dilution with water vapour H_2O and carbon dioxide CO_2 on the structure and stability of a methane/enriched air premix flame, confined and swirled at atmospheric pressure was studied. Measurements were carried out at constant adiabatic temperature (1773, 1873, 1973 and 2073 K), from air to oxycombustion (enrichment OI ranging from 21 to 100%), for two inlet temperatures (T_0= 373K and 473K), at constant equivalence ratio maintained at 0.91 and inlet aerodynamic conditions maintained constant: average inlet velocity at 30 $m.s^{-1}$ and geometric swirl number at Sn=0.90. The experimental setup is a burner used consisting of a swirled stainless steel single injector, mounted in a combustion chamber operating at atmospheric pressure. The flames were visualized by CH* chemiluminescence. From instantaneous images, the flame contour, detected with a Matlab® processing, was determined. From this flame contour, flame height (H_f) and lift-off height (H_{lo}) were extracted by measuring respectively the maximum height of the flame top and the minimum height of the bottom flame. The evolution of the mean macrostructure of the flame was then studied. The results of the steam dilution were detailed and compared with those obtained with carbon dioxide. Links between the laminar flame speed and the flame structure and stability were clearly established.

Keywords

Swirling flames of methane/dioxygen-enriched air, flame structure, stability of turbulent flames

1. Introduction

Pending a real energy transition, it is likely that world energy production will remain, in the coming decades, mainly from combustion processes. To reduce greenhouse gas emissions to the atmosphere, two solutions can be considered and implemented while reducing pollutant emissions (NOx, CO, particulate matter, etc.) [1,2]: i) the use of "decarbonated" fuels; ii) capturing carbon dioxide and then sequestering or using it. In both cases, the different techniques associated with them lead to unconventional combustions that are still poorly controlled. The lack of sufficient knowledge of these combustion methods can become a limitation to the development of these technologies and their exploitation. To remove these scientific locks, it is therefore necessary to characterize these combustions not only in a macroscopic way (burner operability, flame instability, pollutant emissions, combustion temperature) but also in a more detailed way (flame structure, flame speed,...) in order to understand the new phenomena involved.

The optimization of CO_2 capture processes usually leads to modifying combustion conditions in order to pre-concentrate the flue gases into carbon dioxide before their capture. The proven and ultimate reference technique is the oxy-combustion technique combined with a recirculation of its flue gases (CO_2) to control combustion temperatures. Its major disadvantage is the high cost of producing pure oxygen, which makes its use, for massive CO_2 capture, economically prohibitive. More economically viable hybrid techniques combining the use of oxygen-enriched air (OEA) at a much lower cost, exhaust gas recirculation (EGR (CO_2, H_2O and N_2)) and CO_2 capture by membrane process have been proposed [3,4]. In the present paper, this new premixed combustion mode ($CH_4/O_2/(CO_2/H_2O)/N_2$) is studied from an experimental point of view, from the simplest conditions to the complex conditions encountered in the industry. Indeed, a study, in laminar mode [5,6], and in turbulent mode (this paper), of the effects of oxygen enrichment of the air and recirculation of flue gases (via the study of dilution by CO_2 and H_2O) on the combustion of premixed natural gas flames in a gas turbine configuration was carried out. The present paper focuses on the experimental study of the premixed combustion of a $CH_4/(CO_2/H_2O)/O_2/N_2$ mixture in a gas turbine configuration. The scientific approach consists in showing and interpreting the links between the fundamental parameters measured and calculated previously [5] on academic flames and the measurements taken on a flame close to industrial operating conditions. Links between the laminar flame speed and the flame structure and stability have already been shown by [7] for low CO_2 dilution. In this publication, the understanding of these links in the case of suroxygenated combustion and highly diluted in CO_2 and H_2O has been conducted. The chosen configuration is a confined swirled premixed flame. The input parameters are the initial temperature T_0, the adiabatic combustion temperature T_{adiab} , the H_2O or CO_2 dilution rate and the oxygen enrichment.

A review of the existing literature on the effects of dilution of recirculation gases via CO_2 and H_2O dilution on swirled flames of CH_4/air and/or CH_4/O_2 shows that the vast majority of studies have focused on the effects of dilution with CO_2. Watanabe et al. (2016) [8] and Jourdaine et al. (2016) [9] compared swirled CH_4/air flames with CH_4/O_2 flames diluted in CO_2. Watanabe et al. (2016) [8] found that the overall length of CH_4/air flames is greater than that of CH_4/O_2 flames diluted in CO_2, producing a 17% difference between the two. They attributed this behaviour to the chemical effect of CO_2 dilution on the reaction rate of the reactive mixture. In contrast, Jourdaine et al. (2016) [9] concluded that by using the same adiabatic flame temperature, richness and thermal power in the burner, CH_4/air and CH_4/O_2 flames diluted in CO_2 produce similar flame shapes and are placed in the same position. The effects of CO_2 dilution on the swirled flame structure of CH_4/O_2 were also studied by Li et al. (2017) [10]. The authors concluded that the CO_2 dilution (about 70% in the O_2/CO_2

mixture) did not alter the flame structure with respect to CH_4/air flames. Khalil & Gupta (2017) [11] studied CH_4/O_2 flame fluctuations as a function of CO_2 dilution. Their results showed that CO_2 dilution remarkably helps to stabilize swirled oxy-flames, keeping all flame fluctuations below 60 Hz. Nemitallah et al. (2018) [12] also demonstrated stability of methane oxy-flames with the presence of CO_2 in the reactive mixture, concluding that the change in the macrostructure of the flame can be controlled mainly with the entry velocity of the mixture. Abdelwahid et al. (2018) [13] recently attributed these changes to the macrostructure (length and shape) of CH_4/O_2 flames diluted in CO_2, due to a change in reaction rate in the combustion zone.

Compared to studies on CO_2 dilution, studies describing water vapour dilution are very few. Richards et al. (2004) [14] compared the effects of H_2O dilution with CO_2 dilution on swirled CH_4/O_2 flames. The authors showed that the use of water vapour compared to carbon dioxide reduced the residence time by a factor of 5 to 7 to oxidize CO to CO_2. For a constant combustion chamber size, the consequence is that the CO level at equilibrium is much higher with the CO_2 diluent than with H_2O. Göke et al. (2013) [15] studied the effects of water vapour dilution on swirled CH_4/air flames. The authors concluded that flames obtained under wet conditions were more stable and reduced the risk of flashback. The shape and size of the swirled flames diluted with water vapour were studied by Terhaar et al. (2014) [16] and Li et al. (2017) [10] who concluded that the introduction of water caused significant changes in the position and structure of the flame, from a stable V-shaped attached flame to a completely detached annular flame. Lellek and Sattelmayer (2017) [17] and Cadavid et al. (2018) [18] found that in addition to controlling and stabilizing swirled flames, water vapour dilution controlled the flame temperature, resulting in reduced pollutant emissions, mainly NO.

In this paper, the results and analyses of the experimental study characterizing the effect of dilution with water vapour and then with carbon dioxide on the structure, stability, chemiluminescence, flame velocity of a confined premix flame swirled at atmospheric pressure are presented. In a first part, the flame conditions are given. Then, the experimental set-up as well as the measurement techniques and associated diagnostics are described. In a third part, the results of the steam dilution are detailed and the comparison of the results between the dilution with carbon dioxide and that with water vapour is given. Finally, in the last part, the effect of excess air, *e* (or equivalence ratio, ϕ) is presented. This study thus aims at contributing to a technological and socio-economic challenge: the development of CO_2 capture processes for zero-emission energy systems.

2. Flame conditions

In this study, the effect of the mole fraction of diluent X_{H2O} (or X_{CO2}) and of the oxygen enrichment of air (OI, eq. 1) are carried out by keeping constant the inlet temperature T_0 and the adiabatic flame temperature T_{adiab}. For that, four adiabatic flame temperatures (T_{adiab}=1773, 1873, 1973 and 2073K) compatible ωith the operation and thermal stresses of current gas turbines [19], and two inlet temperatures (T_0= 373K and 473K), avoiding the water condensation and representing the effect of compressor heating (in the gas turbine condition), were tested.

For all the tests, the aerodynamic input conditions were kept constant: chamber pressure, P_0 at 0.1MPa, bulk velocity U_b at 30 $m.s^{-1}$ and geometric swirl number S_n at 0.9. In addition, all the tests were carried out with a constant equivalence ratio of ϕ = 0.91 (eq. 2) corresponding to a constant excess of oxygen (*e* = 0.1, eq. 3) low enough to minimize the consumption of enriched air [3] while allowing "complete" combustion. As a result, the methane flow rate (i.e. thermal power) was

modified at each test condition to meet both the input velocity and the mixing condition. This study was separately carried out for the two diluents H_2O and CO_2.

The matrix of the input conditions is reported in Table 1 (and details are given in table S1 in the supplementary file). The mole fractions of the reactants calculated to achieve the target adiabatic temperature were determined using the Chemical WorkBench code [20] by iteratively calculating the thermodynamic equilibrium under isobaric and adiabatic conditions. For ϕ and OI fixed, $X(CH_4)$, $X(O_2)$ and $X(N_2)$ are linked by equations 1,2,3,4 and 5.

Table 1: Experimental conditions tested for H_2O and CO_2 diluents.

P_0=0.1 MPa			U=30m.s^{-1}	
Diluent	e	T_0 (in K)	T_{adiab} (in K)	OI
H_2O and CO_2	0.10	373 and 473	1773 1873 1973 2073	0.21 - 0.25 - 0.30 - 0.40 - 0.50 - 0.60 - 0.75 - 0.85 - 1.0

The input conditions are expressed by the diluent (H_2O or CO_2), T_0, ϕ, OI, where:

OI, the Oxygen Index of the enriched air: $$OI = \frac{X_{O_2}}{X_{O_2}+X_{N_2}}$$ eq. 1

ϕ, the equivalence ratio: $$\phi = \frac{{X_{CH_4}}/{X_{O_2}}}{\left({X_{CH_4}}/{X_{O_2}}\right)_{stoech}} = 2\frac{X_{CH_4}}{X_{O_2}}$$ eq. 2

e, excess of oxygen: $$e = \frac{1-\phi}{\phi}$$ eq. 3

Molar reactive mixture: $$1CH_4 + \frac{2}{\phi}\left(O_2 + \frac{1-OI}{OI}N_2\right) + aH_2O + bCO_2$$ eq. 4

If a≠0, then b=0. If b≠0, then a=0

Mole fraction of diluent

in the reactive mixture: $$X_{H_2O} = \frac{a}{1+\frac{2}{\phi}\frac{1}{OI}+a} \text{ or } X_{CO_2} = \frac{b}{1+\frac{2}{\phi}\frac{1}{OI}+b}$$ eq. 5

The resulting values of the mole fractions of the reactants (O_2, N_2, H_2O and CO_2) are reported in Fig.1 for all the tested conditions. Thanks to equation 2, the mole fraction of CH_4 can be calculated from the mole fraction of O_2.

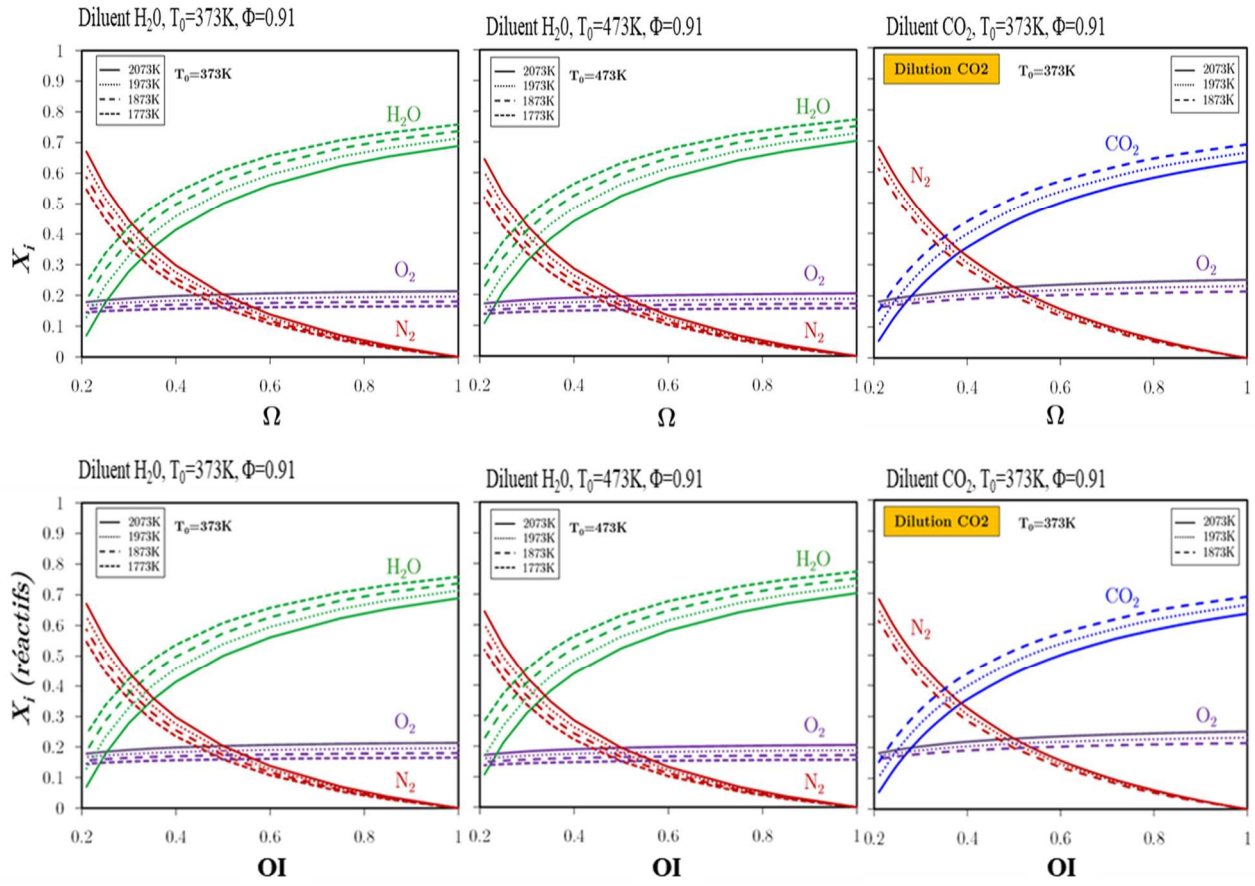

Figure 1: Mole fraction of the reactive mixture (with OI: the quality of the enriched air; ϕ: the equivalence ratio, T_0: the initial temperature).

3. Material and methods

3.1. Experimental set-up

The burner used in this study consists of a swirled stainless steel single injector, mounted in a combustion chamber operating at atmospheric pressure (Fig.2).

Fig. 3 shows the burner with its different components. It consists of a square section of 100 mm² and 250 mm high. Three sides of the combustion chamber are equipped with a quartz window (250 x 78 mm²) providing large optical access for non-intrusive optical measurements. The fourth side corresponds to a metal wall on which the ignition system is implemented at a height of 100 mm from the bottom of the chamber. A plenum located under the combustion chamber is used in order to homogenize and laminarize the gas mixture ($CH_4/O_2/N_2/H_2O/CO_2$) at the inlet of the axial swirler that fed the combustion chamber. In order to eliminate the parasitic dilution with ambient air that could be induced by the central depression of the swirled flow, the burner outlet section is reduced by a

convergent. Inlet and outlet temperatures of the combustion chamber are measured by two type K thermocouples. The uprights of the chamber structure are cooled by a water flow.

The outer diameter (D_{out}) of the axial swirler is 18 mm. The swirler (Fig. 3) consists of six 1 mm thick helical blades, which are attached to a central solid cylinder 8 mm (D_{in}) in diameter, forming the central "bluff-body" at the exit of the injector. The angle of the blade (50°) is chosen in order to obtain a swirl number above the critical value of 0.6 leading to a flow with a central recirculation zone [21]. Its calculation from the geometrical expression of Huang et al. (2009) [22]: $S_n = \frac{2}{3}\left(\frac{1-(D_{out}/D_{in})^3}{1-(D_{out}/D_{in})^2}\right)$ gives a swirl number S_n=0.90.

The gases supply to the burner are provided by gas cylinders for each pure species ($CH_4/O_2/N_2/CO_2$). The water vapour flow is produced by a steam generator developed at laboratory. It consists of a cylindrical vessel whose bottom is made of a metal (copper) with very good thermal conductivity. This bottom is heated by 12 electric heating cartridges with a total power of 7.2kW corresponding to a maximum steam flow rate of 10 $kg.h^{-1}$. The copper plate bottom is maintained at a temperature higher than the boiling temperature and lower than the calefaction temperature of the water allowing the best heat exchange coefficient during evaporation and allowing a good temporal stability of steam flow rate. The water steam flow rate is indirectly controlled by the liquid water inlet flow rate, which is then sprayed and “continuously” evaporated on the hot plate. In order to prevent the steam condensation phenomena, the walls of the vessel and pipes are electrically heated and insulated, moreover a nitrogen flow is injected in the vessel in order to reduce the saturation pressure of water.

Water vapour and gases are introduced into a first mixer equipped with baffles, then into an electric heater (4kW-Inline-OSRAM) in order to reach the T_0 inlet temperature. For safety reasons, the methane is injected in a last mixer at the electric heater outlet. All flowmeters and the heater are controlled by a LabView interface, ensuring the injection flow rates and the inlet temperature required for each working condition (Fig.2). The volume flow rate of the reactive mixture was kept constant at the burner inlet in order to maintain constant the bulk velocity (U_b =30 $m.s^{-1}$.) at the exit of the axial swirler.

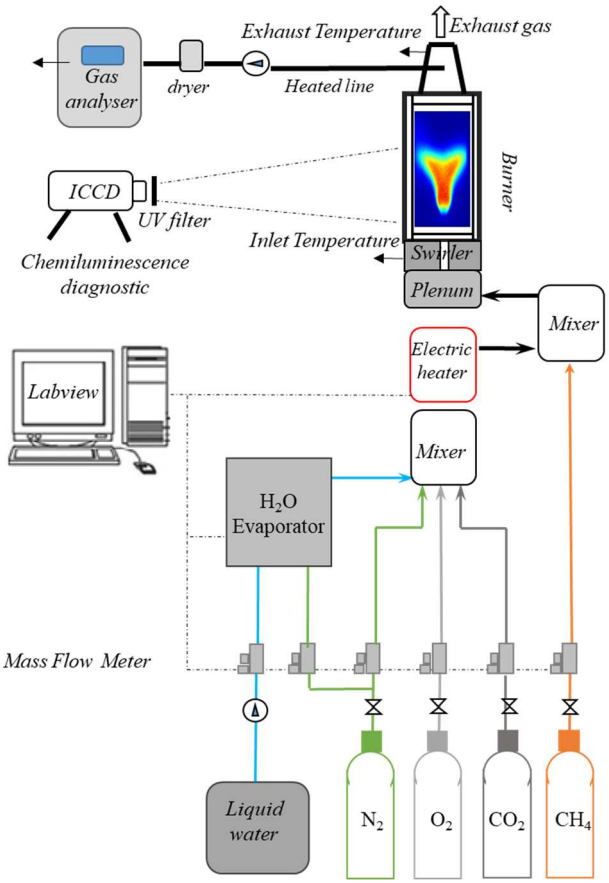

Figure 2: Schematic of the experimental set-up.

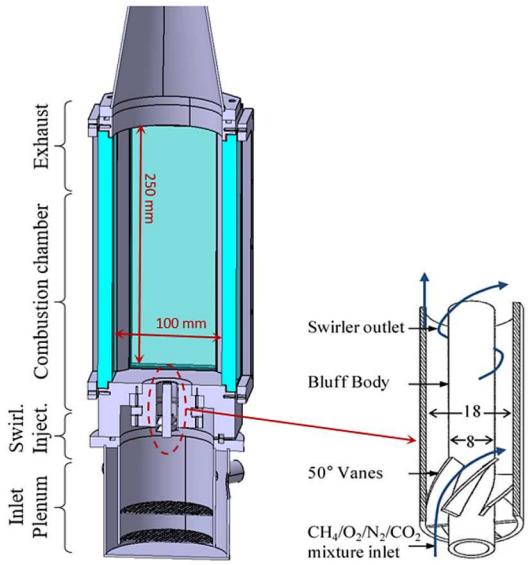

Figure 3: Schematic of the swirl Burner.

3.2. Measurement techniques and associated diagnostics

The flame chemiluminescence is detected using a 16-bit Princeton Instrument CCD intensified camera (PI-MAX Gen II) with a Nikkor 105 mm (f/4.5) UV lens. The camera has a 1024 x 1024 pixel² sensor and the measurement field was 153 x 153 mm² leading to a spatial resolution of 6.69 pix/mm. The CH* emission was filtered using a bandpass filter centered at 430 nm with a 20 nm bandwidth. The exposure time and gain are kept constant during all measurements: 2.5 ms and 100 respectively. For each working condition, 500 instantaneous images (Fig. 4a) are collected at a frequency of 5 Hz in order to obtain relevant statistics (mean and RMS) (Fig. 4c).

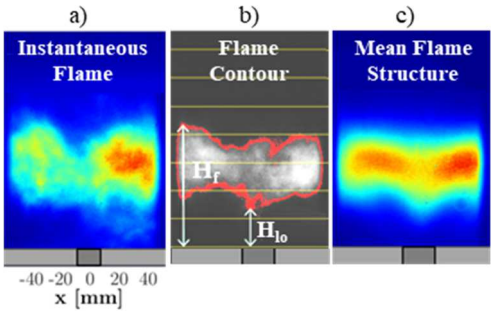

Figure 4: Examples of data processing from CH* chemiluminescence images: a) Instantaneous images of CH* chemiluminescence. b) Contour extraction of the instantaneous image, determination of the flame height (H_f) and the flame Lift-Off H_{lo}. c) Mean Flame Structure calculated from 500 instantaneous images.

From instantaneous images, the flame contour (red line – see Fig. 4b) is detected with a Matlab® processing by following a chosen intensity threshold. From this flame contour, flame height (H_f) and lift-off height (H_{lo}) can be extracted by measuring respectively the maximum height of the flame top and the minimum height of the bottom flame.

4. Study of swirled flames diluted with water vapour

4.1. Topology and chemiluminescence

Fig. 5a shows the average images of the 500 instantaneous chemiluminescence images of CH* obtained in the $CH_4/O_2/N_2/H_2O$ flames under all conditions described in the first line of Table 1. In order to properly visualize and compare the flame structure, all the average images are presented by adapting the maximum scale in order to obtain all the colour dynamics. These images cannot therefore be compared to each other in terms of signal strength. However, to allow a quantitative comparison, the maximum average intensity $\overline{CH^*_{\max}}$ (corresponding to the red color of each mean image in Fig.5a) is reported in Fig.5b as a function of OI.

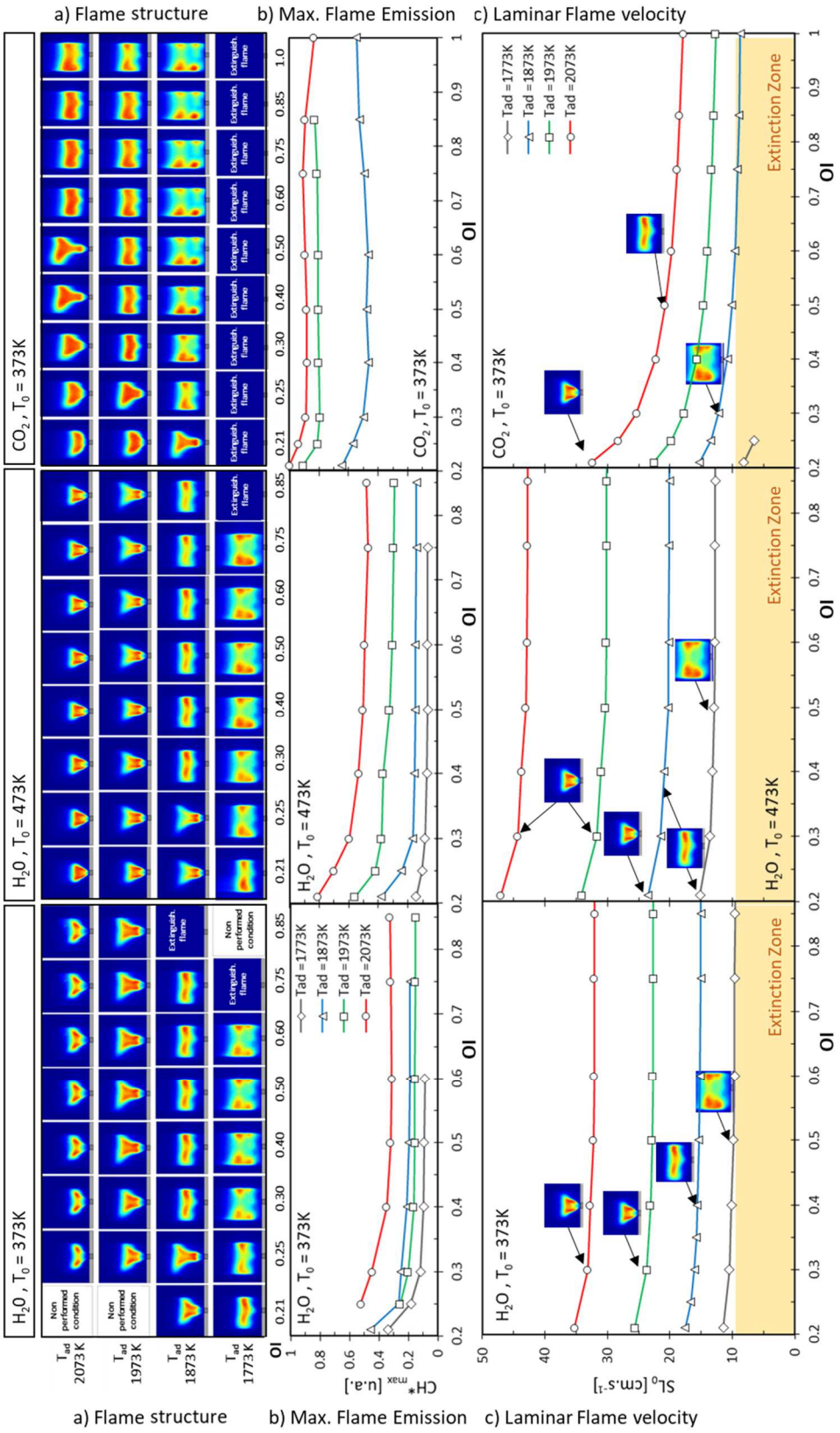

Figure 5: Experimental and calculated results for the 3 different reactive mixtures (T_0 = 373K, H_2O), (T_0 = 473K, H_2O) and (T_0 = 373K, CO_2) as a function of the enrichment parameter OI and of the adiabatic flame temperature T_{ad}. a) Mean CH* Flame Structure, b) Mean global intensity of CH* chemiluminescence, c) calculated laminar flame velocity. (P_0=1atm, φ=0.91, U_b =30 m.s^{-1}.)

In Fig. 5a, the evolution of the mean macrostructure of the flame can be observed:

- from left to right, when the oxygen index OI increases, i.e. as the air nitrogen is replaced by water vapour (see Fig.1) for constant initial temperature T_0 and adiabatic flame temperature T_{adiab} conditions;

- from top to bottom, when the adiabatic flame temperature decreases.

a) Flame shape

The flame generated by this swirl burner can take 3 forms which are shown in Fig. 6:

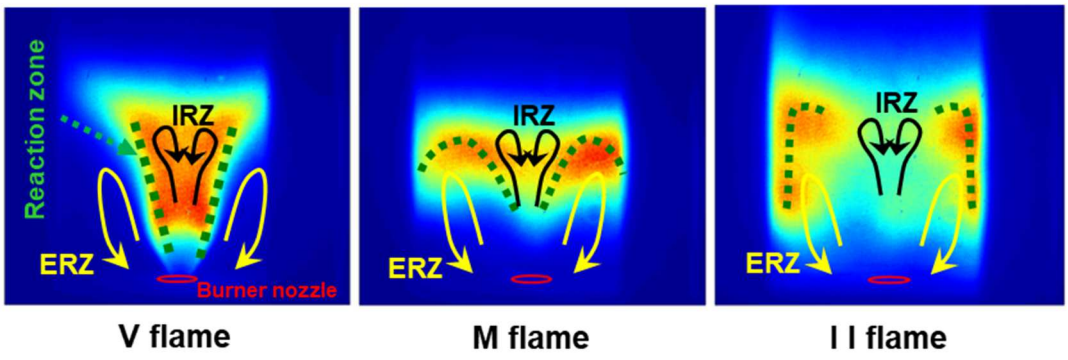

Figure 6: Presentation of the three mean flame structures (V, M and I I)

- *"V" flame*: The flame is anchored at the outlet of the injector and flared into a V- shape in the combustion chamber. The reaction zone occurs within the limits of the internal shear layer (ISL) of the reactive mixture in contact with the internal recirculation zone (IRZ). This type of flame has been obtained for adiabatic flame temperatures of 2073 and 1973 K. As the oxygen enrichment OI increases, the "V" extends upwards from the burner and the angle of the "V" decreases.

- *"M" flame*: The reaction zone still occurs in the ISL, but the flame is now detached from the burner nozzle. The swirling flame is stabilized and lifted at a height H_{lo} above the burner. The reactive zone spreads up to the external recirculation zone (ERZ), along the walls, giving the flame the shape of an M. For water dilution, this type of flame was obtained at adiabatic flame temperatures of 1873K.

- *"I I" flame*: Combustion no longer takes place in the central part of the flame but only in the ERZ still along the walls. In this condition, the flame extends quite far downstream of the burner. The flame is also the site of instability. This type of flame was obtained at adiabatic flame temperatures of 1773 K. For lower adiabatic temperatures or higher dilutions the flame is extinguished.

b) Flame height (H_f) and Lift-Off height (H_{lo})

The mean and the RMS measurements of the flame height (H_f) and of the lift-off height (H_{lo}) are performed from 500 instantaneous CH* emission images as shown in Fig.7 as a function of OI and for each adiabatic temperature condition.

It can be noted that the lift-off height (H_{lo}) is exactly 0 for conditions T_{adiab} = 1973 and 2073 K, which corresponds to a stable V-shaped flame attachment to the burner nose (Fig. 7, bottom). For the condition T_{adiab} = 1873 K, the M flame is detached and this results in a H_{lo} ranging from 25 to 30 mm for the condition T_0=373K (respectively from 15 to 30 mm at T_0 = 473 K). As shown by the standard deviation bars, this lifted flame leads to fluctuations in its height, which indicates a relatively unstable character of this flame. At T_0 = 373 K, the standard deviation varies from 12 to 15 mm when OI increases (respectively from 9 to 15 mm at T_0 =473K). For the I I flame condition at T_{adiab} = 1773 K, there is an increase of the lift-off height (H_{lo}) from 28 to 38 mm for the condition T_0 = 373 K (respectively from 23 to 40 mm at T_0 = 473 K). The most remarkable fact for this type of flame in I I is the very clear increase in the fluctuations of the position of the foot of the flame, thus demonstrating a very unstable character of this flame especially for the high values of enrichment OI. The fluctuation values are almost double those observed for the V flame condition. They increase from 13 to 27 mm for both conditions T_0=373 and 473 K.

Concerning the flame heights (H_f) (Fig. 7, top), there is an overall increase in the flame height as the adiabatic flame temperature decreases. However, this is not entirely true for the cases of T_{adiab} = 1973 and 1873 K and can be explained by the fact that the flame lifting between these two temperatures artificially induces a jump on the height of the resulting flame. The flame height fluctuations for the stable V-shaped flame are no longer negligible as were those of the lift-off height and can be estimated at 10 mm for the flame at T_{adiab} =2073 K, T_0 =373 and 473K. For T_{ad} = 1973K, the fluctuations increase from 8 to 12 mm and 10 to 20 mm respectively for T_0=373 and 473 K. For the M flame, the same order of magnitude of fluctuations can be observed. For the I I flame, its instability is again observed by the strong fluctuations in flame height which increase up to 30 mm when the enrichment Ω increases. In addition, beyond OI =0.6 at T_0 = 373 (respectively 0.75 at 473 K), the flame is extinguished. This extinction phenomenon has already been observed by Lafay et al. (2007) on the same burner in lean combustion conditions, i. e. in the case of high dilution with air. As Bradley et al. (1998) [23] and Coriton et al. (2013) [24] have shown, this extinction can be explained by a decrease in the flame resistance to stretching. These flame topologies are consistent with those observed by Terhaar et al. (2014) [16], who experimentally evaluated the effects of H_2O dilution on swirled methane flames. They attributed the transition from a V-type flame to an M-type flame to the high dilution rates of water vapour. These results are also consistent with those reported by Huang and Yang (2004) [25] and Yin et al. (2017) [26], who observed changes in flame topology from a 100 K variation in the preheating temperature of the reactive mixture.

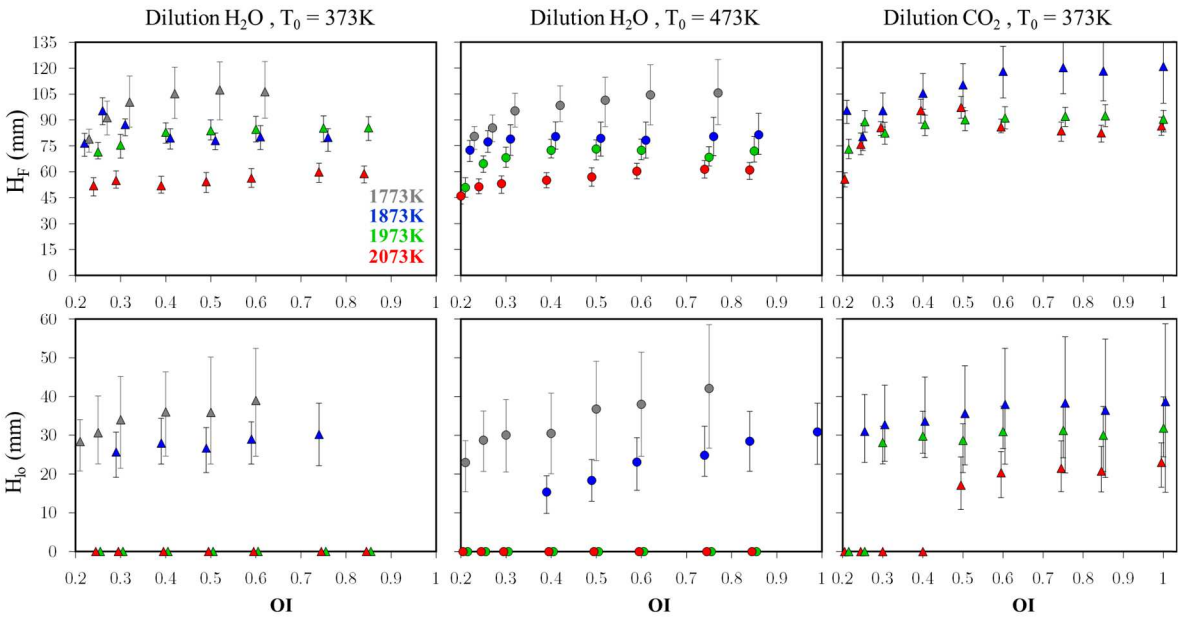

Figure 7: a) Flame height H_f , b) Lift-Off Height of the flame H_{lo}, for the 3 different reactive mixtures (T_0 = 373K, H_2O), (T_0 = 473K, H_2O) and (T_0 = 373K, CO_2) as a function of the enrichment parameter OI and of the adiabatic flame temperature T_{ad}. (P_0=1atm, φ=0.91, U_b =30 m.s^{-1}.). Bars represent the standard deviations of H_{lo} and H_f.

c) Summary

Overall (see Fig. 5-7), it can be noticed that the flames stabilized at higher adiabatic temperatures and slightly water diluted (lower enrichment) are very compact and anchored as close as possible to the burner outlet. As the H_2O dilution (or OI Oxygen Index) and the initial temperature T_0 increase and especially as the adiabatic temperature T_{ad} decreases, there is a change in the structure of the flame which results in:

- a change of shape (Fig. 5a, Fig. 6);

- an overall increase of flame height (H_f) (Fig. 7);

- an increase of lift-off height (H_{lo}) (Fig.7);

- a destabilization of the flame (Fig. 7);

- a decrease of the spontaneous emission intensity of the CH* radical (Fig. 5b).

4.2. Correlation with laminar flame speed

In Fig. 5c, the evolution of the laminar flame velocity is represented. It was calculated using the CWB code [20] and the reaction mechanism GRIMech.3.0 [27] as extensively described in [5] for all the flame conditions represented in Fig. 5 for two initial temperatures T_0= 373 and 473 K and four adiabatic temperatures T_{adiab} = 1773, 1873, 1973 and 2073 K as a function of oxygen index (OI). Overall, it can be noticed that the laminar flame velocity decreases when the initial T_0 and adiabatic T_{adiab} temperatures decrease and to a lesser extent when Ω increases. The maximum value of the flame velocity is

47 cm.s^{-1} @ (473 K, 2073 K, OI =0.21) and the minimum value is 10 cm.s^{-1} @ (373K, 1773K, OI =0.85), close to the extinction conditions of this burner [7] shown in yellow in Fig. 5c. For the highest adiabatic temperature conditions (2073 and 1973 K), the sensitivities at the initial temperature T_0 and the adiabatic temperature T_{adiab} are approximately identical since a decrease of 100 K implies a speed reduction of about 11 cm.s^{-1} for the flame at T_0 = 473 K and T_{adiab} = 2073 K and 10 cm.s^{-1} for that at T_0 = 473 K, T_{adiab} = 1973 K. These sensitivities decrease when adiabatic temperature decreases. At T_{adiab} = 1773 K, the sensitivity to adiabatic temperature becomes preponderant compared to the initial temperature, it is about twice as high here (8.5 versus 4 cm.s^{-1}).

It is also possible to observe correlation between the laminar flame velocity (Fig. 5c) and the macrostructure of the flame (Fig. 5a). Stable V flames are encountered at high flames speeds (greater than 25 cm.s^{-1}). It is this high velocity that allows them to be anchored to the burner nozzle and also the consumption of reactants over a short length along the internal shear layer. Below 25 cm.s^{-1}, the low flame speeds no longer allow the flame to be anchored to the burner. The foot of the flame is then convected downstream of the injector and returns to a fluctuating stabilization position a little higher in the ISL where flow velocities are lower. In addition, low flame velocities induce the end of reagent consumption much further downstream in the ISL and can even occur in external recirculation zones, along the wall of the furnace leading to the M shape. Finally, for low speeds (<15 cm.s^{-1}), the flame no longer finds a stable position in the ISL due to significant stretching and is pushed towards areas with low stretching and low flow velocity along the walls. For very low speeds (<10 cm.s^{-1}), fluctuations induce very high local extinctions which statistically lead to total extinction.

5. Comparison of H_2O and CO_2 dilution

In this section, a comparative analysis between the dilution with CO_2 and the flames diluted with H_2O vapour is presented for the case T_0 = 373 K. The comparison of the input conditions (see Fig.1) shows that for the same condition (U_b, T_0, T_{adiab}), the mole fraction of CO_2 is always slightly lower than that of H_2O. This is especially due to the highest calorific capacity of CO_2 (Fig 8). Consequently, the maintaining of the total volume flow rate of the reactive mixture lead to a methane flow rate greater in the case of CO_2 dilution than in the case of H_2O dilution.

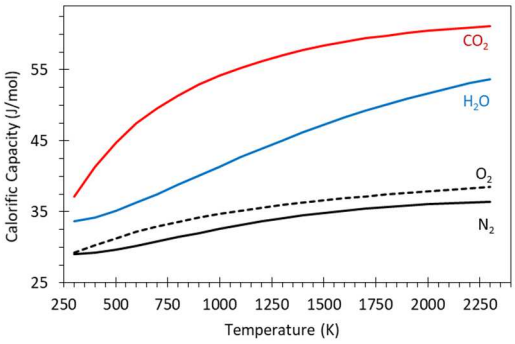

Figure 8: Heat molar capacity of CO_2, H_2O, N_2 and O_2 as a function of the temperature

Fig. 5a shows the average chemiluminescence CH* images of the $CH_4/O_2/N_2/H_2O/CO_2$ mixture, as a function of OI, for the four adiabatic flame temperatures studied (1773, 1873, 1973 and 2073 K) and the two inlet temperatures : T_0 = 373 and 473 K in the case of dilution with CO_2 and dilution with H_2O. It can be seen that the three types of flames (V, M and I I) are observed in the case of CO_2

dilution as well as H_2O water vapour dilution. Nevertheless, the shape of flames differ according to the diluent for the same condition (OI, T_0, T_{adiab}). For example, for CO_2 dilution, we observe that at high adiabatic temperatures (2073 K), the M-type flame appears for the high OI and that the I-type flame appears from 1873 K. This is not observed with the dilution in water vapour H_2O for which these two types of flames do not exist. It can also be noted that in the case of dilution with carbon dioxide CO_2, it was not possible, for the lowest adiabatic temperature (1773 K), to stabilize the flame in the combustion chamber (the flame was systematic extinguished).

As shown in [5] for low CO_2 dilution, laminar flame speed seems to be a fundamental combustion parameter that drives the flame structure. In our case, this is clearly shown in Fig. 5a and 5c, where the laminar flame velocities and flame structure are simultaneously compared for the two diluents H_2O and CO_2 according to OI and to adiabatic flame temperature (T_{adiab}). From Fig. 5 onwards, the following remarks can be made:

-In the case of H_2O dilution and for a constant T_{ad}, the laminar flame velocity decreases slowly when OI increases and meanwhile, the flame structure evolves slowly. Whereas, in the case of CO_2 and especially for low enrichment values dilution, the laminar flame velocity decreases quite sharply when OI increases which leads to a significant change of the flame structure.

-For the same condition (OI, T_0, T_{adiab}) the laminar flame velocity in the case of CO_2 dilution is always lower than thus in the case of H_2O dilution. For the high values of OI, the difference in flame speed is about 15 $cm.s^{-1}$ for T_{ad} = 2073 K and only 7 $cm.s^{-1}$ for 1873 K. The consequence is that the replacement of H_2O by CO_2 modifies significantly the flame structure. In the case of CO_2 dilution and at T_{adiab}=1773 K the laminar flame velocity is always small enough (< 10 $cm.s^{-1}$.) to avoid the stabilization of the flame (the combustion was not possible) whereas in the same conditions the combustion was possible with H_2O dilution.

As the lift-off height (H_{lo}) and flame heights (H_f) are dependent on the flame structure, significant differences between the dilution of CO_2 and H_2O for the same condition can be observed (Fig. 7). However, if we refer to the same flame structure between the two diluents, the heights and their respective fluctuations (instabilities) become equivalent.

All these results are summarized for the two diluting conditions (H_2O and CO_2) in Fig. 9, where laminar flame speed, the mean flame structure and the flame stability are plotted as a function of the flame adiabatic temperature and as a function of OI.

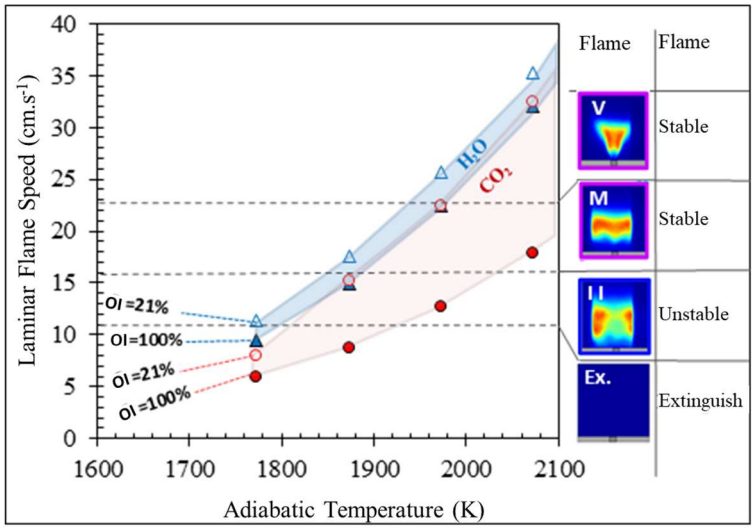

Figure 9: Evolution of laminar flame speed, mean flame structure and flame stability as a function of flame adiabatic temperature and OI for the diluting conditions (H_2O and CO_2). (T_0 = 373K, P_0=1atm, ϕ=0.91, U_b =30 m.s^{-1}.)

It can be observed that for the two diluents (H_2O, CO_2) the structure and the stability of the flame depend only on the laminar speed of the flame. It is noteworthy, that for the H_2O diluent the flame velocity depends mainly on the flame adiabatic temperature whereas for the CO_2 diluent the flame velocity depends both on the adiabatic flame temperature T_{ad} and on the air enrichment OI.

6. Conclusion

In this paper, the effect of water vapour and carbon dioxide dilution on the structure, stability, and laminar flame velocity of a confined, premixed and $CH_4/O_2/H_2O/CO_2/N_2$ flame at atmospheric pressure were presented. The measurements were carried out in a confined premixed flame swirl burner operating at atmospheric pressure. Measurements were made at constant adiabatic temperature (1773, 1873, 1973 and 2073 K), in methane flames, from air to oxycombustion (Oxygen Index ranging from 21 to 100%), for two inlet temperatures (T_0= 373K and 473K), with an equivalence ratio maintained constant at 0.91. The input aerodynamic conditions were kept constant at the following values: an average velocity of 30 m.s^{-1} and a geometric swirl number of Sn=0.90. The results of the water vapour dilution were detailed and compared to those obtained with carbon dioxide. Whatever the diluent H_2O and CO_2, it has been clearly demonstrated that the structure and stability of the flame is mainly related to the velocity of the laminar flame, which depends only on the initial mixing conditions, the temperature and pressure of the reactive mixture, i.e. the oxygen index OI, the equivalence ratio ϕ, the preheating temperature (T_0), the adiabatic temperature (T_{adiab}) and the nature of the diluent.

Three main types of flame structures were observed:

- V Flame : For the highest laminar flame velocity (up to 23 cm.s^{-1}), the flame is short and highly anchored to the central bluff body of the injector. The flame takes the form of a V.
- - M Flame - For an intermediate laminar flame speed from 16 to 23 cm.s^{-1}, the decrease in laminar flame speed prevents the flame from anchoring to the burner corresponding to the upper stretch zone. The flame is then lifted above the burner and the reaction zone is convected to the corner recirculation zone. Then the flame takes the form of an M and is relatively unstable.

- II Flame - For a low laminar flame speed from 11 to 16 $cm.s^{-1}$, combustion is only possible in the low stretch area corresponding to the corner recirculation area, leading to a flame shape I I. This flame mode is very unstable and leads to local extinction.
- A lower laminar flame speed causes the burner to be completely extinguished.

In general, oxy-fuel combustion is a way to increase the efficiency of the CO_2 capture process, but for thermal reasons this combustion must be strongly diluted by exhaust gases, pure CO_2 or steam. In existing methane/air swirled burners (e. g. gas turbine combustor), flame structure and stability are adapted by modifying the equivalence ratio, it can be concluded that oxy-combustion could be used with an existing swirl burner without changing the burner and combustion chamber geometries by controlling only the flame velocity with the dilution ratio (Exhaust gas recirculation ratio). Since flame temperature control is also a main parameter in the design of the combustion chamber, it is observed that in the case of H_2O dilution, the choice of laminar flame speed determines the adiabatic flame temperature. On the contrary in the case of CO_2 dilution, for a constant laminar flame velocity, the temperature of the adiabatic flame increases as the oxygen index increases (CO_2 dilution increases). This phenomenon could be a disadvantage of CO_2 dilution compared to water dilution.

References

[1] Barmaa M.C, R. Saidurb, S.M.A. Rahmand, A. Allouhie, B.A. Akashf, S. M. Saitg (2017). A review on boilers energy use, energy savings, and emissions reductions. Renewable and Sustainable Energy Reviews, vol.79, pp. 970–983.

[2] Kohse-Höinghaus K (2018). Clean combustion: Chemistry and diagnostics for a systems approachin transportation and energy conversion. Progress in Energy and Combustion Science, vol. 65, pp. 1-5.

[3] Belaissaoui B, G. Cabot, M. S. Cabot, D. Willson, E. Favre (2013). CO2 capture for gas turbines: an integrated energy-efficient process combining combustion in oxygen-enriched air, flue gas recirculation, and membrane separation. Chemical Engineering Science, vol. 97, pp. 256-263.

[4] Baker R.W, B. Freeman, J. Kniep, X. Wei, T. Merkel (2017). CO2 capture from natural gas power plants using selective exhaust gas recycle membrane designs. International Journal of Greenhouse Gas Control, vol. 66, pp. 35-47.

[5] Chica Cano, J.P., G. Cabot, F. Foucher, S. de Persis (2018). Effects of oxygen enrichment and water dilution on laminar methane flames at high pressure. Fuel, vol.225, pp. 499-508.

[6] Cabot G, J.P. Chica Cano, S. De Persis, F. Foucher (2017). Study of Experimental and Calculated Flame Speed of Methane/Oxygen-Enriched Flame in Gas Turbine Conditions As a Function of Water Dilution: Application to CO2 Capture by Membrane Processes. In ASME Turbo Expo 2017: Turbomachinery Technical Conference and Exposition. American Society of Mechanical Engineers.

[7] Lafay Y, B. Taupin, G. Martins, G. Cabot, B. Renou, A. Boukhalfa (2007). Experi-mental study of biogas combustion using a gas turbine configuration. Experi-ments in fluids, vol.43, pp. 395-410.

[8] Watanabe. H., S. J. Shanbhogue, S. Taamallah, N. W. Chakroun, A. F. Ghoniem (2016). The structure of swirl-stabilized turbulent premixed CH4/air and CH4/O2/CO2 flames and mechanisms of intense burning of oxy-flames. Combustion and Flame, vol. 174, pp. 111–119.

[9] Jourdaine. P., C. Mirat, J. Caudal, A. Lo, T. Schuller (2016). A comparison between the stabilization of premixed swirling CO2-diluted methane oxy-flames and methane/air flames. Fuel, vol. 201, pp. 156–164.

[10] Li. M., Y. Tong, M. Thern, J. Klingmann (2017). Investigation of methane oxy-fuel combustion in a swirl-stabilised gas turbine model combustor. Energies, vol.10, pp. 648.

[11] Khalil. A.E.E., and A. K. Gupta (2017). Flame fluctuations in Oxy-CO2-methane mixtures in swirl assisted distributed combustion. Applied Energy, vol. 204, pp. 303–317.

[12] Nemitallah, S. Alkhaldi, A. Abdelhafez, M. Habib (2018). Effect analysis on the macrostructure and static stability limits of oxy-methane flames in a premixed swirl combustor. Energy, vol.159, pp. 86-96.

[13] Abdelwahid. S., Nemitallah, M., Imteyaz, B., Abdelhafez, A., & Habib, M. (2018). Effects of H2 Enrichment and Inlet Velocity on Stability Limits and Shape of CH4/H2–O2/CO2 Flames in a Premixed Swirl Combustor. Energy & Fuels, 32(9), pp. 9916-9925.

[14] Richards. G.A., K. H. Casleton, B. T. Chorpening (2004). CO2 and H2O diluted oxy-fuel combustion for zero-emission power. Proceedings of the Institution of Mechanical Engineers, Part A: Journal of Power and Energy, vol. 219, pp. 121 – 126.

[15] Göke. S., M. Füri, G. Bourque, B. Bobusch, K. Göckeler, O. Krüger,,.. & C.O. Paschereit (2013). Influence of steam dilution on the combustion of natural gas and hydrogen in premixed and rich-quench-lean combustors. Fuel processing technology, vol. 107, pp. 14-22.

[16] Terhaar. S., K. Oberleithner, C.O. Paschereit (2014). Impact of steam-dilution on the flame shape and coherent structures in swirl-stabilized combustors. Combustion Sci-ence and Technology, vol. 186(7), pp. 889-911.

[17] Lellek S, T. Sattelmayer (2017). NOx formation and CO burnout in water injected, premixed natural gas flame as typical gas turbinecombustor residennce time. Proceedings of ASME Turbo Expo. June 26-30, 2017, Charlotte, NC, USA.

[18] Cadavid. Y., A. Amell, J. Alzate, G. Bermejo, G.A. Ebratt (2018). Analysis of Water–Fuel Ratio Variation in a Gas Turbine With a Wet-Compressor System by Change in Fuel Composition. Journal of Engineering for Gas Turbines and Power, vol. 140(5), 052602.

[19] Cordier. M., A. Vandel, G. Cabot, B. Renou, and A. M. Boukhalfa (2013). Laser induced spark ignition of premixed confined swirled flames. Combustion Science and Technology, vol. 185, pp. 379–407.

[20] Deminsky M., V Chorkov, G Belov, I Cheshigin, A Knizhnik, E Shulakova, M Shulakov, I Iskandarova, V Alexandrov, A Petrusev, I Kirillov, M Strelkova, S Umanski, B Potapkin (2003). Chemical Workbench––integrated environment for materials science. Computational Materials Science, vol. 28, pp. 169-178.

[21] Gupta, A.K., D. Lilley, and N. Syred (1993). Swirl flows. Abacus Press, Cambridge.

[22] Huang, Y., V. Yang (2009). Dynamics and stability of lean-premixed swirl-stabilized combustion. Progress in Energy and Combustion Science, vol. 35 (4).

[23] Bradley D., R. a. Hicks, M. Lawes, C. G. W. Sheppard, and R. Woolley (1998). The measurement of laminar burning velocities and Markstein numbers for iso-octane-air and iso-octane-nheptane-air mixtures at elevated temperatures and pressures in an explosion bomb. Combustion and Flame, vol. 115, pp. 126–144.

[24] Coriton. B., J. H. Frank, A. Gomez (2013). Effects of strain rate, turbulence, reactant stoichiometry and heat losses on the interaction of turbulent premixed flames with stoichiometric counterflowing combustion products. Combustion and Flame, vol. 160, pp. 2442 – 2456.

[25] Huang. Y., V Yang (2004). Bifurcation of flame structure in a lean-premixed swirl-stabilized combustor: transition from stable to unstable flame. Combustion and Flame, vol. 136, p.p. 383-389.

[26] Yin. Z., P. Nau, W. Meier (2017). Responses of combustor surface temperature to flame shape transitions in a turbulent bi-stable swirl flame. Experimental Thermal and Fluid Science, vol. 82, pp. 50–57.

[27] SMITH G.P, D. M. GOLDEN, M. FRENKLACH, N. W. MORIARTY, B. EITENEER, M. GOLDENBERG, C. T. BOWMAN, R. K. HANSON, S. SONG, W. C. GARDINER, JR., VITALI V. LISSIANSKI, AND ZHIWEI Q (1998) GRIMECH3.0 IN HTTP://WWW.ME.BERKELEY.EDU/GRI_MECH/.

Acknowledgements

The research leading to these results received funding from the COCC program in France through the support of the EMC3Labex and Caprysses Labex.